View metadata, citation and similar papers at core.ac.uk
brought to you by CORE
provided by HKU Scholars Hub

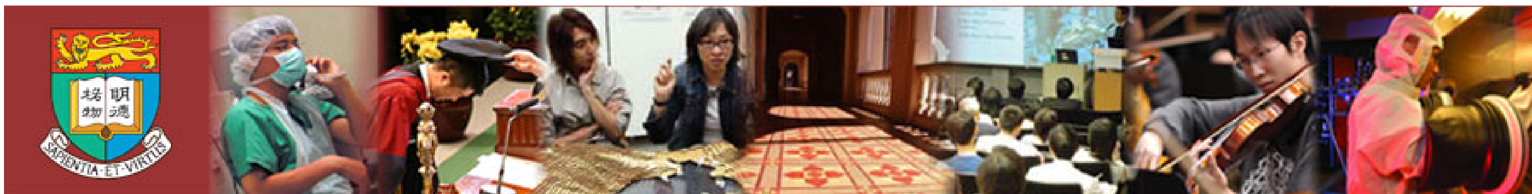

Title	Thermal evolution of defects in undoped zinc oxide grown by pulsed laser deposition
Author(s)	WANG, Z; Su, S; Ling, FCC; Anwand, W; Wagner, A
Citation	Journal of Applied Physics, 2014, v. 116, p. 033508
Issued Date	2014
URL	http://hdl.handle.net/10722/199208
Rights	Creative Commons: Attribution 3.0 Hong Kong License

JOURNAL OF APPLIED PHYSICS 116, 033508 (2014)

Thermal evolution of defects in undoped zinc oxide grown by pulsed laser deposition

Zilan Wang,[1] Shichen Su,[1] Francis Chi-Chung Ling,[1,a)] W. Anwand,[2] and A. Wagner[2]
[1]*Department of Physics, The University of Hong Kong, Pokfulam Road, Hong Kong, People's Republic of China*
[2]*Institute of Radiation Physics, Helmholtz-Zentrum Dresden-Rossendorf, Bautzner Landstr. 400, 01328 Dresden, Germany*

(Received 13 May 2014; accepted 5 July 2014; published online 16 July 2014)

Undoped ZnO films are grown by pulsed laser deposition on c-plane sapphire with different oxygen pressures. Thermal evolutions of defects in the ZnO films are studied by secondary ion mass spectroscopy (SIMS), Raman spectroscopy, and positron annihilation spectroscopy (PAS), and with the electrical properties characterized by the room temperature Hall measurement. Oxygen deficient defect related Raman lines 560 cm^{-1} and 584 cm^{-1} are identified and their origins are discussed. Thermal annealing induces extensive Zn out-diffusion at the ZnO/sapphire interface and leaves out Zn-vacancy in the ZnO film. Two types of Zn-vacancy related defects with different microstructures are identified in the films. One of them dominates in the samples grown without oxygen. Annealing the sample grown without oxygen or growing the samples in oxygen would favor the Zn-vacancy with another microstructure, and this Zn-vacancy defect persists after 1100 °C annealing. © *2014 AIP Publishing LLC*. [http://dx.doi.org/10.1063/1.4890460]

I. INTRODUCTION

ZnO has been received great deal of attention in the past 10 years because of its excellent physical properties for fabricating optoelectronic devices.[1] Defects in semiconductors play crucial role in determining the materials optical and electrical properties. The realization of practical ZnO-based devices is still suffering from the asymmetric p-type doping difficulty of ZnO,[2,3] which is also at least partially related to the poor understandings of the defects, defect compensation, and defect control in the ZnO materials.

There have been theoretical studies on the defects of ZnO but the results are dependent on the approach, approximation, and post-process adopted (Refs. 4–7 and references therein). It is generally accepted that Zn vacancy is a double acceptor having energy states $\varepsilon(0/-1)$ and $\varepsilon(-1/-2)$ at 0.1–0.2 eV and 0.9–1.2 eV above the valence band, respectively. The calculated formation energy of V_{Zn} is high in p-type ZnO and it decreases with the E_F moving towards the conduction band. V_{Zn} is the important residual acceptor in n-type ZnO material. Oxygen vacancy is generally agreed to be a deep negative U donor with the state $\varepsilon(0/2+)$ calculated to be 0.4–0.8 eV. It has low formation energy for p-type ZnO, but the calculation results show divergence on whether V_O exists in n-type ZnO. Zn interstitial is a shallow donor. It is mobile at low temperature because of its low migration barrier. The oxygen interstitial exists in two configurations namely the octahedral configuration and the tetrahedral split configuration. The octahedral configuration has two deep acceptors states, but its formation energy is high in equilibrium situation. The split configuration has lower formation energy but it is electrically inactive. Zn-antisite has the calculated high formation energy for n-type ZnO. The calculated formation energy for the oxygen antisite is high and is not expected to exist in equilibrium situation.

Experimental defect study of ZnO has been performed using a variety of spectroscopic techniques like positron annihilation spectroscopy (PAS),[8–15] photoluminescence (PL),[16–21] and Raman spectroscopy (RS).[22–26] PAS is selectively sensitive to V_{Zn} related defects. V_{Zn} (Refs. 8–10) and V_{Zn}-hydrogen complexes[12] have been identified in n-type ZnO. PAS has also been used to study the different Zn-vacancy related phenomena like the thermal induced formation and the dissociation of the shallow acceptor in As-doped ZnO,[13,14] the residual donor responsible for the n-type conductivity in undoped ZnO,[15] etc. Broad defect emission bands with different wavelengths are frequently observed in ZnO materials. Among these defect emissions with different colors, green luminescence (GL) is commonly observed but its origin is controversial. It has been ascribed to Cu impurity,[16] Zn-vacancy,[17] O-vacancy,[18] O-antisite (O_{Zn}),[20] Zn interstitial complex,[21] etc. Two Raman modes of 584 cm^{-1} (E_1-LO) and 560 cm^{-1} were reported to be defect related and have been associated to O-vacancy and Zn-interstitial, respectively.[22–26]

In the present study, defects in pulsed laser deposition (PLD) grown undoped ZnO films are investigated by a variety of spectroscopy methods, including PAS, Raman spectroscopy, and secondary ion mass spectroscopy (SIMS). The effects of growth stoichiometry and post-growth annealing are systemically studied.

II. EXPERIMENTAL

Undoped ZnO films were grown by the PLD method on the c-plane sapphire substrate. The ZnO target is obtained from the Kurt J. Lesker Co. (purity of 99.999%). The

a)Author to whom correspondence should be addressed. Electronic mail: ccling@hku.hk

 © 2014 AIP Publishing LLC

[This article is copyrighted as indicated in the article. Reuse of AIP content is subject to the terms at: http://scitation.aip.org/termsconditions. Downloaded to] IP: 147.8.31.43 On: Mon, 26 Jan 2015 04:38:15

background pressure of the growth chamber is 1×10^{-4} Pa. To study the effect of growth stoichiometry, the growth was carried out with three different oxygen pressures, namely, $PO_2 = 0$ Pa, 1.3 Pa, and 5 Pa. During the growth, 248 nm laser pulse from the Coherent COMPexPro 102 excimer laser was used. The pulse energy and repetition rate of the laser pulse are 300 mJ and 2 Hz, respectively. The substrate temperature was kept at 300 °C during the growth. The isochronal annealing process was conducted in a tube furnace in the Ar atmosphere for 30 min at different annealing temperatures T_{anneal} up to 1100 °C. For the atomic force microscopic study, the ZnO samples are covered with and without another piece of ZnO in the Ar atmosphere to investigate the effect on the surface roughness. For the other spectroscopic measurements, the ZnO samples are annealed open to the Ar atmosphere without cover. The Hall measurement was conducted at room temperature using the van der Pauw configuration by the Accenet HL-5500PC system. X-ray diffraction measurement was performed using the Bruker D8 Advance x-ray diffractometer with the Cu Kα line (0.1541 nm). The SIMS measurement was conducted using the Cameca (Model IMS 4F) dynamic secondary ion mass spectrometer. The Raman measurement was carried out using a WITec-Alpha con-focal micro-Raman system under the back scattering geometric configuration. The excitation source is a 514.5 nm Ar laser with an output power of 30 mW. The laser beam is focused onto the sample with a 60× objective. Atomic force microscope (AFM) measurement is carried out to investigate the morphology using the Asylum Research MFP3D in semi-contact (tapping) mode.

PAS measurement was carried out using a 25 keV mono-energetic positron beam as the positron source. The annihilation gamma ray energy spectrum is collected using a high purity Ge detector and the corresponding nuclear electronic, which has an energy resolution of 1.3 keV for the 514 keV line. The Doppler broadening of the annihilation gamma photons is monitored by the S- and W-parameters, which are defined as the ratios of the central window count, and the summation of the two wings count to the total count of the annihilation peak, respectively. The window for the S-parameter is 511 ± 0.76 keV, and those for the W-parameter are 511 ± 3.4 keV and 511 ± 6.8 keV. Experimental details of the PAS measurement can be found in Ref. 13. For the case of ZnO, the PAS parameters (i.e., the S and W parameters) are selectively sensitive to V_{Zn} and its related complex.

III. RESULTS AND DISCUSSIONS

Figures 1(a) and 1(b) show the AFM images of the oxygen free grown samples in the as-grown state and after the 900 °C annealing open to Ar atmosphere, respectively. The surface of the 900 °C annealed sample is damaged, but damage is not found in samples annealed at 750 °C. The surface roughness of the as-grown sample is 1.97 nm and that after the 900 °C covered annealing increases to 3.37 nm. With the aim to reduce the surface damage and improve the roughness, we have covered another piece of ZnO on top of the sample during the 900 °C annealing process and the AFM image was shown in Figure 1(c). No surface damage is found and the surface roughness reduces to 0.82 nm.

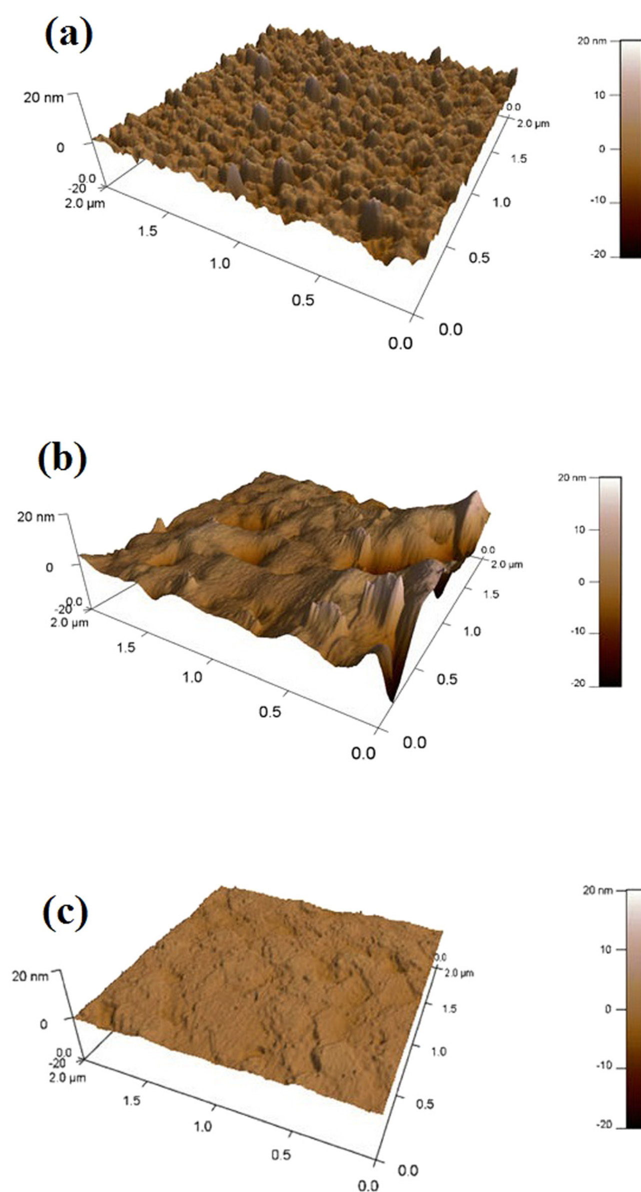

FIG. 1. AFM pictures showing the morphology of the ZnO samples: (a) as-grown; (b) annealed at 900 °C with the cover of another piece of ZnO; and (c) annealed at 900 °C without the cover of another piece of ZnO. The samples are grown with the oxygen pressure of 0 Pa.

XRD measurements have been carried out on the samples grown at the PO_2 of 0 Pa and 5 Pa. Three peaks are identified in all the XRD spectra, namely, peaking at 34.5°, 41.7°, and 72.1° and being associated with ZnO (002), sapphire (006), and ZnO (004), respectively. Figure 2 shows the region of the XRD spectra containing the Zn (002) and sapphire (006) peaks for the samples grown at PO_2 of 0 Pa and annealed at different temperature. This indicates that the grown ZnO film has the single-phase wurtzite structure with the c-axis as the preferential orientation. Figure 3 shows the full-width-half-maximum (FWHM) of the ZnO (002) peaks against the annealing temperature for the samples with PO_2 equal to 0 Pa and 5 Pa. The FWHM decreases with the annealing temperature, indicating the improvement of the

[This article is copyrighted as indicated in the article. Reuse of AIP content is subject to the terms at: http://scitation.aip.org/termsconditions. Downloaded to] IP: 147.8.31.43 On: Mon, 26 Jan 2015 04:38:15

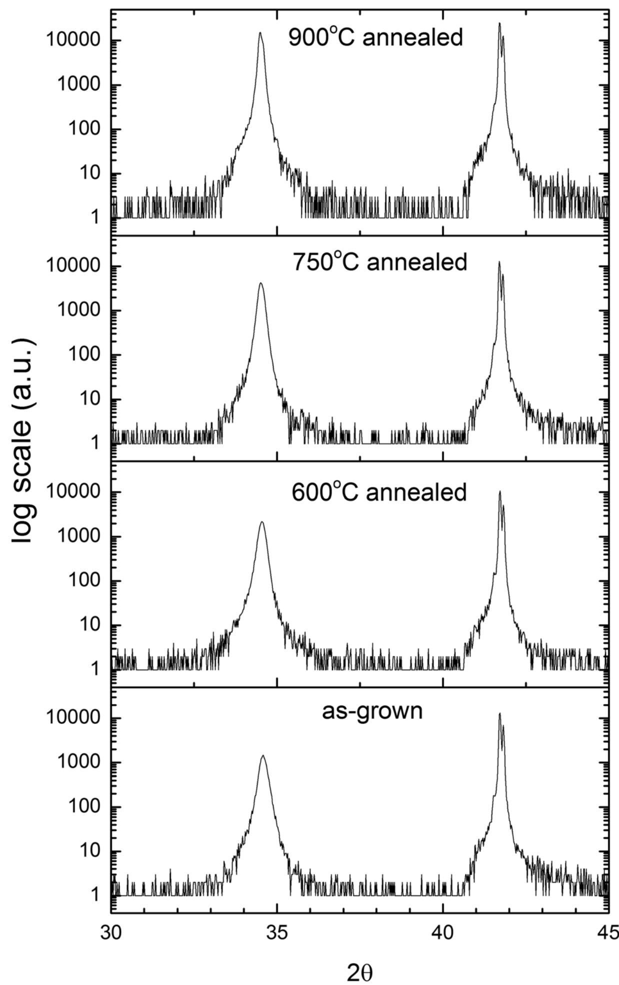

FIG. 2. The ZnO (002) and sapphire (600) peaks as found in the XRD spectra for the samples grown at the substrate temperature of 300 °C with 0 Pa oxygen pressure undergone different annealing temperatures.

crystalline quality. At the annealing temperature of 900 °C, the FWHM reaches value of ~0.12°, irrespective of the initial growth oxygen pressure.

Figure 4 shows the electron concentrations as a function of the annealing temperature for the ZnO samples grown at

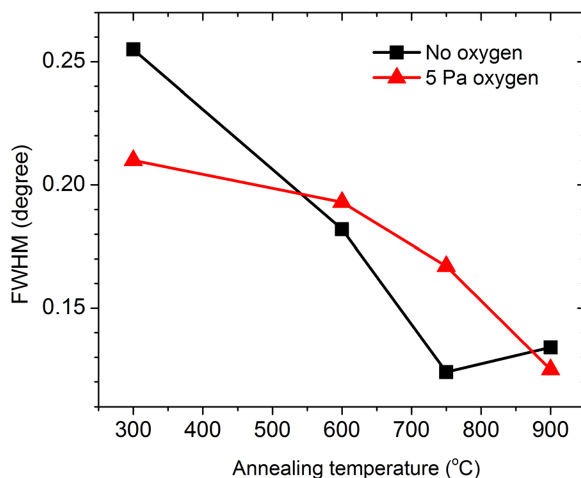

FIG. 3. The FWHM of the ZnO (002) peaks as a function of the annealing temperature. The samples are grown at the substrate temperature of 300 °C in the oxygen pressures of 0 Pa and 5 Pa.

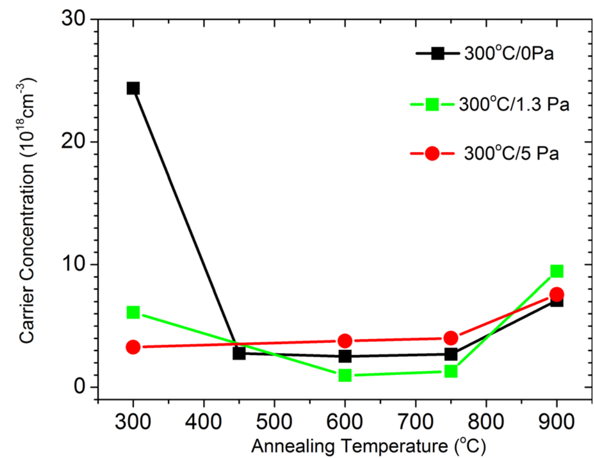

FIG. 4. The data of the electron concentration against the annealing temperature for the ZnO samples grown with the oxygen pressures of 0 Pa, 1.3 Pa, and 5 Pa.

PO_2 of 0 Pa, 1.3 Pa, and 5 Pa. The as-grown sample grown with no oxygen has electron concentration of 2×10^{19} cm^{-3}. For the other two samples grown with oxygen, the as-grown electron concentrations are ~3–6 × 10^{18} cm^{-3}, which are significantly lower than that grown without oxygen. Irrespective of the oxygen pressure during growth, all the three samples have electron concentrations laying in a relatively narrow range of 1–6 × 10^{18} cm^{-3} for the annealing temperature range between 450 °C and 750 °C. For all the samples, further annealing up to 900 °C would have the effect of slightly increasing the electron concentration, reaching values of 7–9 × 10^{18} cm^{-3}. The three as-grown samples have the mobility of ~20–30 cm^2 V^{-1} s^{-1} and have the maximum mobility achieved after the 900 °C annealing with the values of 95 cm^2 V^{-1} s^{-1}, 50 cm^2 V^{-1} s^{-1}, and 85 cm^2 V^{-1} s^{-1} for the samples grown at $PO_2 = 0$, 1.3, and 5 Pa, respectively.

To monitor for the hydrogen in the ZnO film as well as the Zn and Al inter-diffusion at the ZnO/sapphire interface, SIMS measurements were conducted on the samples grown with $PO_2 = 0$ Pa and 1.3 Pa, and upon the post-growth annealing with different temperatures. Figures 5 and 6, respectively, show the SIMS depth profiles of Zn, Al, and H for the samples grown with $PO_2 = 0$ Pa and 1.3 Pa annealed at different temperatures. Hydrogen is found throughout the ZnO film in all the samples. The H concentrations were calculated using a control undoped ZnO sample implanted by H with known fluence and energy, and with the SIMS signal intensity calibrated against the H concentration obtained by the Monte Carlo TRIM[27] code. The thus calculated H concentrations of the PLD grown ZnO samples against the annealing temperature are shown in Figure 7. The as-grown sample grown at 1.3 Pa oxygen pressure has higher H-concentration than that grown without oxygen (2.5×10^{19} cm^{-3} and 1.2×10^{19} cm^{-3}, respectively). After the 600 °C annealing, the H-concentrations of both sets of the samples dropped significantly to the similar value of ~8 × 10^{18} cm^{-3}. They then decreased very slightly after the 900 °C annealing.

For both the samples grown with $PO_2 = 0$ and 1.3 Pa, the inter-diffusions of Al and Zn across the ZnO/sapphire interfaces in the as-grown samples are with the depth of

[This article is copyrighted as indicated in the article. Reuse of AIP content is subject to the terms at: http://scitation.aip.org/termsconditions. Downloaded to] IP: 147.8.31.43 On: Mon, 26 Jan 2015 04:38:15

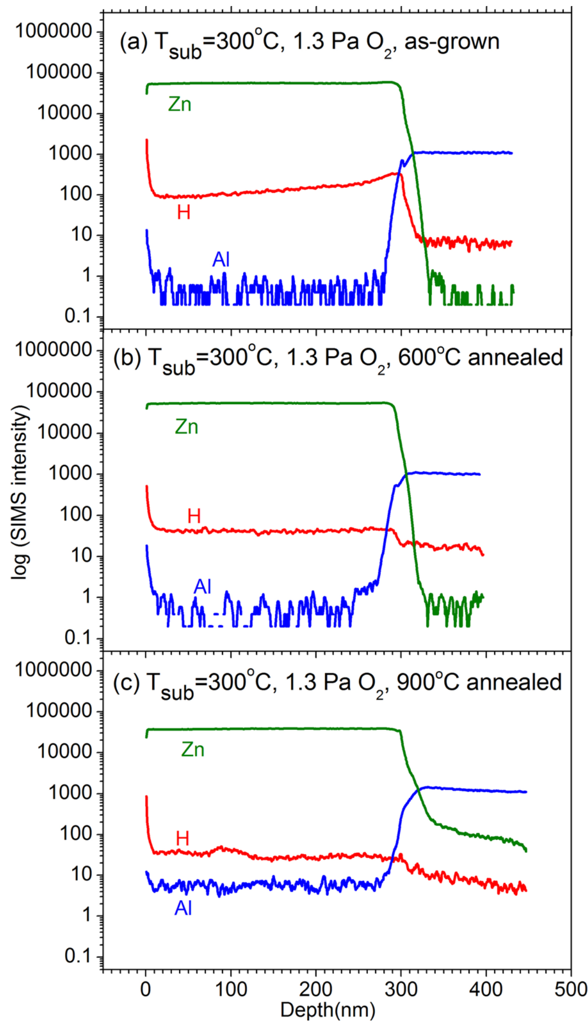

FIG. 5. The SIMS depth profiles of H, Zn, and Al of the (a) as-grown; (b) 600 °C annealed; and (c) 900 °C annealed samples grown without oxygen.

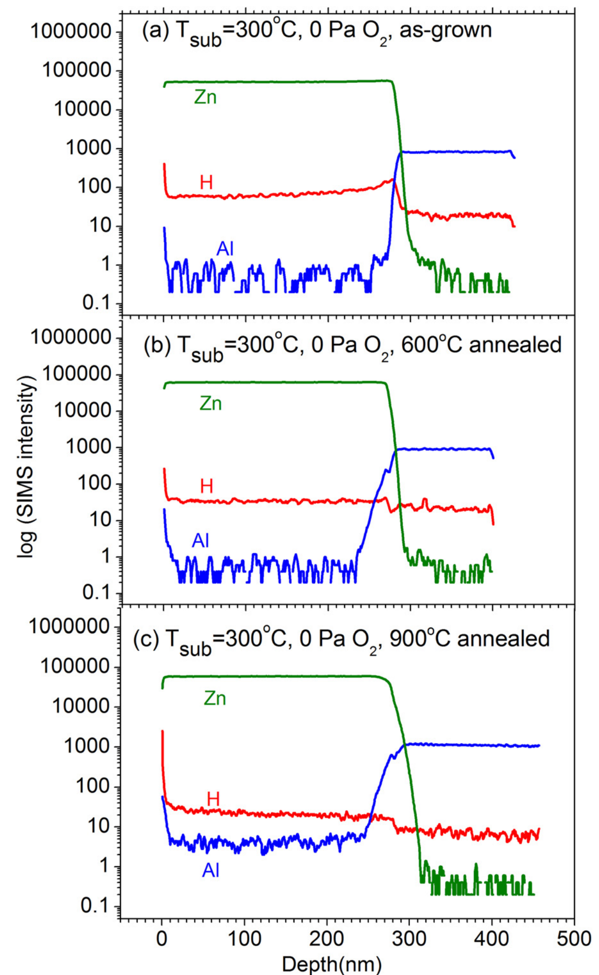

FIG. 6. The SIMS depth profiles of H, Zn, and Al of the (a) as-grown; (b) 600 °C annealed; and (c) 900 °C annealed samples grown with oxygen pressure of 1.3 Pa.

~30 nm (Figure 5 and 6). After the 600 °C annealing, the inter-diffusion depths of Al and Zn slightly increase to ~30–40 nm. The 900 °C thermal annealing induced Zn out-diffusion from the ZnO film is very different for the samples grown with and without oxygen during the growth. For the sample grown without oxygen, the ZnO/sapphire interface is relatively stable, with the diffusion depths of Al and Zn increased to 50 nm and 40 nm, respectively, after the 900 °C annealing. However, for the sample grown at 1.3 Pa oxygen pressure, there is extensive Zn diffusion into the sapphire substrate with the depth of ~100 nm after the 900 °C annealing. The Al diffusion depth is similar to that found in the sample grown without oxygen, i.e., equal to ~50 nm. It is unclear why the sample grown with oxygen has more extensive Zn out-diffusion from the ZnO film, and further study is needed.

Hydrogen has been attributed to be the residual shallow donor associated with the n-type conduction in undoped ZnO.[28] It would be worthwhile to compare the thermal evolution of the H-concentrations and the electron concentrations to understand the carrier conduction in the present samples. For the as-grown samples, the sample grown with oxygen has higher H-concentration but lower electron

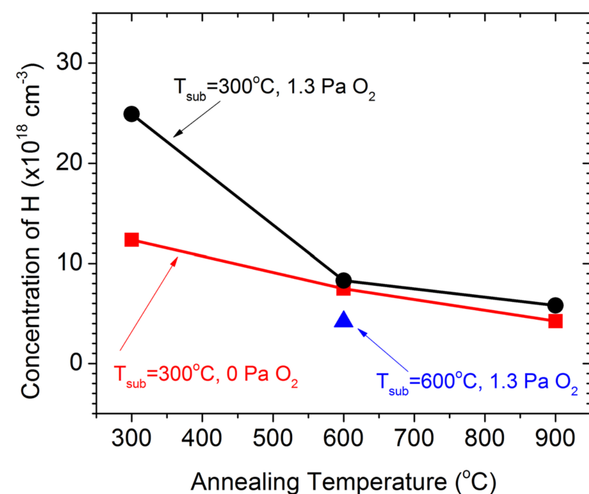

FIG. 7. The hydrogen concentration as a function of the annealing temperature for the samples grown with oxygen pressures of 0 Pa and 1.3 Pa at the substrate temperature of 300 °C. The hydrogen concentration of the as-grown sample grown with 1.3 Pa oxygen pressure and 600 °C substrate temperature is also included.

[This article is copyrighted as indicated in the article. Reuse of AIP content is subject to the terms at: http://scitation.aip.org/termsconditions. Downloaded to] IP: 147.8.31.43 On: Mon, 26 Jan 2015 04:38:15

concentration than those grown without oxygen (Figures 4 and 7). The low electron concentration found in the H abundant sample grown in oxygen could be due to the inferior crystalline quality as revealed by the FWHM of the ZnO (002) XRD peak (Figure 3). The H concentrations for all the samples annealed at 600 °C lay within narrow range of ∼4–8 $\times 10^{18}$ cm^{-3} (Figure 6). Irrespective of the initial growth conditions, the electron concentrations of all the samples annealed at 600 °C lays within the narrow range of 1–4 $\times 10^{18}$ cm^{-3}, which is close to that of the hydrogen concentration. It is plausible to suggest that hydrogen impurity is the important shallow donor responsible for the n-type conduction for the samples undergone the 600 °C annealing. Comparing the H concentration and electron concentration (Figures 4 and 7), the slight increase of electron concentration after the 900 °C annealing is not related to the hydrogen impurity.

Figure 8 shows the Raman spectra of the ZnO samples grown without oxygen undergone the 600 °C and 900 °C annealing in the Raman shift range of 490 cm^{-1} to 610 cm^{-1}. Raman peaks of 584 cm^{-1} and 560 cm^{-1} have, respectively, been associated to the intrinsic defects of V_O and Zn_i.[22–26] The broad Raman peak as seen in the 600 °C annealed sample (Figure 8) could be well fitted with the two intrinsic defect related peaks (560 cm^{-1} and 584 cm^{-1}) in addition with the sapphire substrate related peak (579 cm^{-1}). The resultant fitted curve and the corresponding components' curves are shown in Figure 8. For the Raman spectrum of the 900 °C annealed sample as shown in Figure 8, thermal removal of the two intrinsic defect related peaks are clearly observed, and only the sapphire related peak remains. It would be interesting to investigate the stoichiometry dependence of these defect related Raman peaks. The intensities of the two Raman peaks of the as-grown samples grown with $PO_2 = 0$ Pa, 1.3 Pa, and 5 Pa are tabulated in Table I.

TABLE I. The intensities of the two Raman peaks 560 cm^{-1} and 584 cm^{-1} for the as-grown samples grown at different oxygen pressure. The substrate temperature during growth is 300 °C.

	Intensities of Raman peaks	
Oxygen pressure during growth	560 cm^{-1}	584 cm^{-1}
0 Pa	∼4000	∼500
1.3 Pa	270	3
5 Pa	186	0

Figure 9 summarizes the intensities of the two defect related peaks against the annealing temperature for the samples grown without oxygen. The annealing temperatures of the intrinsic defects associated with the 560 cm^{-1} and 580 cm^{-1} Raman peaks are 750–900 °C and 600–750 °C. Table I clearly demonstrates that the 584 cm^{-1} peak intensity dramatically drops by orders of 100 and 10 000 if the growing environment changes from no oxygen to 1.5 Pa and 5 Pa oxygen, respectively. For the intrinsic defect associated with the 560 cm^{-1} Raman peak, its intensity is less sensitive to the oxygen environment during growth. Its intensity is reduced by about 15 times and 30 times while the growing environment changes from no oxygen to 1.5 Pa and 5 Pa oxygen, respectively. It can be summarized that growing in oxygen environment would suppress the two intrinsic defect related 560 cm^{-1} and 584 cm^{-1} Raman peaks.

The assignment of the 560 cm^{-1} and 584 cm^{-1}, respectively, to Zn_i and V_O as in the previous literatures such as Refs. 22–26 is compatible with the oxygen deficient nature as observed in the present study. V_O is generally believed to have the U-negative property and has the energy state at $\varepsilon(0/2+) = 0.4$–0.8 eV below the conduction band. The Fermi levels calculated from the electron concentration for the present samples are all well above the $\varepsilon(0/2+)$ of V_O, and thus the V_O in the present samples should possess a zero charge state. Janotti and Van de Walle[4] have obtained the theoretical value of 2.36 eV for the migration barrier of neutral V_O^0. This

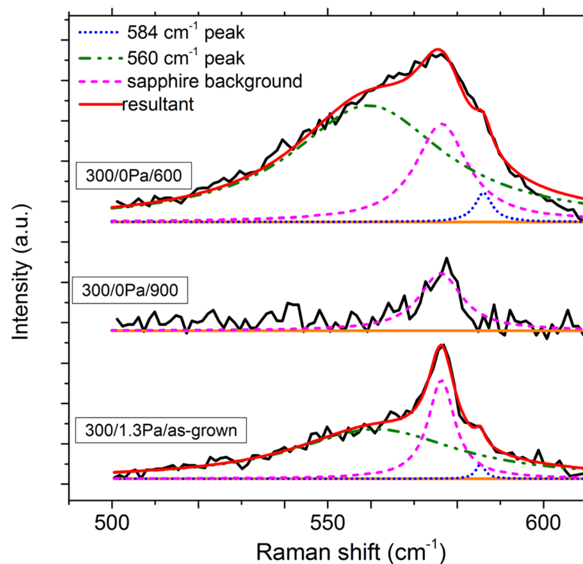

FIG. 8. The Raman spectra of the ZnO samples grown with (a) no oxygen and $T_{anneal} = 600$ °C; (b) no oxygen and $T_{anneal} = 900$ °C; and (c) oxygen pressure of 1.3 Pa and as-grown. The 560 cm^{-1}, 584 cm^{-1} and the sapphire peak are clearly observed in (a). By comparing (a) and (b), 900 °C annealing has the effect of removing the 560 cm^{-1} and 584 cm^{-1} peaks. It is also noticed from (c) that 560 cm^{-1} and 584 cm^{-1} are suppressed by the presence of the oxygen.

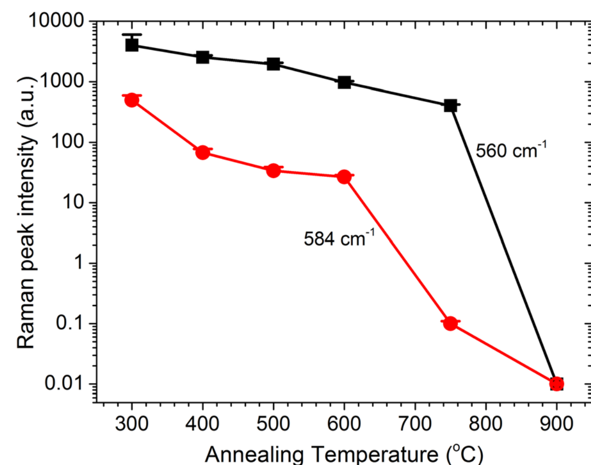

FIG. 9. The intensities of the 560 cm^{-1} and 584 cm^{-1} Raman peaks as a function of the annealing temperature. The Raman peak intensity is in log scale. The samples are grown with no oxygen.

[This article is copyrighted as indicated in the article. Reuse of AIP content is subject to the terms at: http://scitation.aip.org/termsconditions. Downloaded to] IP: 147.8.31.43 On: Mon, 26 Jan 2015 04:38:15

corresponds to the annealing temperature of 909 K, which agrees well with the annealing temperature of the defect associated with the present 584 cm^{-1} Raman peak. The 584 cm^{-1} Raman peaks is thus attributed to the V_O. For the case of Zn_i, theoretical calculation yields the migration barrier of 0.57 eV,[4] which corresponds to the annealing temperature of 219 K. Optically detected magnetic resonance (ODMR) study also shows that the Zn_i anneals out at 170 K.[29] In the present study, the 560 cm^{-1} anneals at temperature of 900 °C, even higher than that of V_O. The assignment of the 560 cm^{-1} Raman peak to Zn_i is thus highly suspicious.

For ZnO materials, PAS technique is selectively sensitive to the Zn-vacancy related defects. To understand the thermal evolution of the V_{Zn}-related defects in the ZnO samples, PAS study was performed on the samples grown with the oxygen pressures of 0 Pa and 5 Pa, and their S-W plots were shown in Figure 10. For the presence of a single type of vacancy defect, the measured resultant S-parameter is the weighted sum of the contributions from the bulk state and the defect state, i.e., $S = (1-\eta)S_b + \eta S_d$,[30] where η is the fraction of the positron annihilating at the defect state, S_b and S_d are the characteristic *S*-parameters of the bulk state and the defect state, respectively. Similar relation holds for the *W*-parameter,[30] $W = (1-\eta)W_b + \eta W_d$. Combining the two equations yields $S - S_b = R(W - W_b)$. This implies in the presence of the single type of positron trapping defect, plotting *S*-parameter against the *W*-parameter would yield a straight line with the slope of *R*. *R* is the characterized *R*-parameter and is a fingerprint of the defect. To normalize against the S_b and W_b, the normalized R_{normal} is given by $R_{normal} = (W_b/S_b)R$.

For the samples grown without oxygen, the *S-W* data points of the as-grown, 400 °C, 500 °C, and 600 °C annealed samples lay on a straight line in the *S-W* plot, implying single type of Zn-vacancy related defect (VZn-1) exists in these samples. For the samples grown at 5 Pa oxygen pressure, the data points lay on another straight line in the S-W plot, implying that another type of Zn-vacancy related defect (VZn-2) exists in these samples. It is noticed that the samples grown without oxygen annealed at 900 °C and 1100 °C also lie on the VZn-2 straight line. The two straight lines intersects at $S_b = 0.5008$ and $W_b = 0.09467$, which are the characteristic S and W parameters of the defect free ZnO bulk state, respectively.

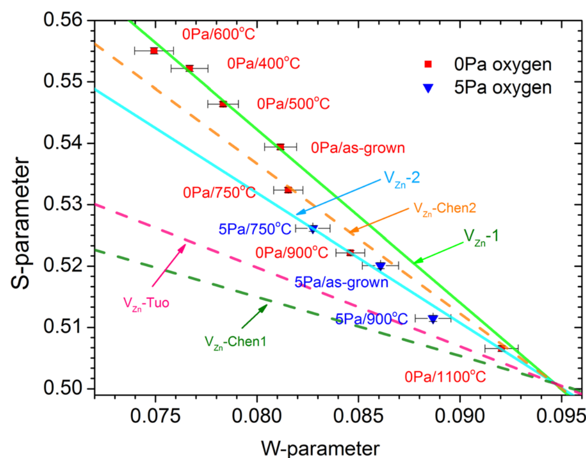

FIG. 10. The S-E parameter plot of the ZnO samples grown with no oxygen (color in red) and 5 Pa oxygen pressure (color in blue). Sample having the same single type of defect would have the S-E data falling on the same straight line. The S-E straight lines corresponding to VZn-1 and VZn-2 are shown. The S-E straight lines for the Zn-vacancy related defects as found in Tuomisto *et al.*[8,9] (VZn-Tuo) and Chen *et al*[10] (VZn-Chen1 and VZn-Chen2) are also included for reference.

The whole picture is that VZn-1 exists in the as-grown sample grown without oxygen. At annealing temperature ≤600 °C, VZn-1 is the only detected Zn-vacancy related defect in the samples. Annealing the samples at 900 °C would initiate the conversion of VZn-1 to another Zn-vacancy related defect VZn-2 with a different microstructure. For the samples grown with 5 Pa oxygen, VZn-2 exists in the as-grown sample as well as the post-growth annealed ones. VZn-2 persists after the 1100 °C annealing.

In the previous paragraph, it has been stated that the slight increase of electron concentrations after the 900 °C annealing was not associated with the hydrogen impurity. As the S-W data points of 0 Pa/750 °C, 0 Pa/900 °C, 5 Pa/750 °C, and 5 Pa/900 °C lay on the straight line of VZn-2 implying the type of Zn-vacancy is the same, their S-parameters are the direct indication of the corresponding Zn-vacancy concentration. From Figure 10, the Zn-vacancy concentrations of the samples grown with and without oxygen drop after the 900 °C annealing. The thermal reduction of the Zn-vacancy compensating center could be the cause for the slight increase of electron concentration after the 900 °C annealing.

Tuomisto *et al.*[8,9] studied the seeded vapor phase grown ZnO bulk using the PAS technique and showed that Zn-vacancy is the dominant acceptor in the as-grown and the electron irradiated samples (denoted by VZn-Tuo). The V_{Zn} has the characteristic fingerprint that the normalized S-parameter and W-parameter of $S_D = 1.039$ and $W_D = 0.87$, and the positron lifetime of 230 ps as compared to the bulk value of 170 ps. Oxygen-vacancy and a negatively charged ion are also identified in the modeled analysis of the PAS data, although their characteristic positron lifetime is close to that of the bulk. The negative ion is attributed to O-interstitial or oxygen antisite. The VZn-Tuo has two annealing stages namely at 400 K and 550 K, indicating that it is part of two different defect complexes. The oxygen vacancy anneals out together with the second annealing stage of V_{Zn}, i.e., 550 K. Chen *et al.*[10] carried out PAS study on electron irradiated hydrothermal grown ZnO bulk samples. Zn-vacancy related defect (denoted by VZn-Chen1) was induced by electron irradiation. Post-irradiation annealing at temperature below ~400 °C would reduce the concentration of VZn-Chen1. Annealing at 400 °C would create another kind of Zn-vacancy related defect (VZn-Chen2). Combining with the Raman scattering result which reveal the presence of oxygen vacancy, the formation of the secondary V_{Zn}-related defect (VZn-Chen2) and the simultaneous annealing out of the V_O Raman signal is attributed to the displacement of the Zn atom neighboring the V_O to the V_O and thus the formation of the $V_{Zn}Zn_O$, i.e., $V_O + Zn_{Zn} \rightarrow V_{Zn}Zn_O$. In a subsequent study of comparing the experimental Doppler broadening of annihilation radiation (DBAR) spectrum with the theoretical one calculated by the local density

[This article is copyrighted as indicated in the article. Reuse of AIP content is subject to the terms at: http://scitation.aip.org/termsconditions. Downloaded to] IP: 147.8.31.43 On: Mon, 26 Jan 2015 04:38:15

approximation model, Chen *et al.*[11] confirmed that the VZn-Chen2 defect is the $V_{Zn}Zn_O$ defect complex.

The characteristic S-W straight lines corresponding to VZn-Tuo, VZn-Chen1, and VZn-Chen2 are included in the present S-W plot (Figure 10) for the purpose of comparison. It is noticed that the VZn-1 and VZn-2 observed in the present study are not the Zn-vacancy related defects observed in the vapor phase grown nor the hydrothermal grown single crystal bulk samples. However, the S-W data point of the 750 °C annealed sample grown without oxygen (denoted by VZn-3) lays on the S-W characteristic line of VZn-Chen2, which is attributed to $V_{Zn}Zn_O$. It coincides with the annealing temperature of the 584 cm^{-1} V_O related Raman line. The same coincidence was also found in the case of the creation of $V_{Zn}Zn_O$ and the disappearance of V_O in the hydrothermal grown ZnO bulk though at the lower temperature of 400 °C, which was ascribed to the $V_O + Zn_{Zn} \rightarrow V_{Zn}Zn_O$ process.[10,11] The S-W data point (i.e., VZn-3) is thus attributed to $V_{Zn}Zn_O$.

It is noticed from Figure 10 that even at temperature as high as 1100 °C, the Zn-vacancy in the PLD grown film has not yet been completely annealed out. This temperature is high as compared to the previously reported annealing temperature of the Zn-vacancy related defects in bulk single crystals, for examples 550 K (i.e., ~280 °C) in vapor phase grown,[9] and 400 °C in hydrothermal grown.[10,31] The extra thermal persistence of Zn-vacancy related defect in the present ZnO films could be due to the thermally fragile ZnO/sapphire interface. Thermal induced inter-diffusions of Al and Zn were observed in the SIMS measurement of the present study, as well as in other literature.[32] The Zn out-diffusion would inevitably create Zn-vacancy related defects in the ZnO film and this could explain the presence of Zn-vacancy related defect in the present samples annealed at temperature as high as 1100 °C. The issue of the thermally fragile ZnO/sapphire interface is important as the thermally induced Zn-vacancy would influence the electrical property of the film, like compensating the p-type conductivity in the p-doping attempt.

From Figures 5 and 6, it is observed that the 900 °C annealing induced Zn out-diffusion from the ZnO film for the sample grown in oxygen is much more extensive than that grown without oxygen. It is thus expected that the Zn-vacancy related defects created by the 900 °C annealing in the sample grown in oxygen is more than that grown without oxygen. From the S-W plot in Figure 10, the S-parameter of the 900 °C annealed samples grown in oxygen is smaller than that grown without oxygen, implying that the Zn vacancy concentration in the 900 °C annealed sample grown with oxygen is less than that grown without oxygen, which is contrary to the expectation. It seems to suggest that Zn-vacancy annealing out in the O-rich sample is more effective. Nevertheless, the exact reason is unknown and requires further investigation.

IV. CONCLUSION

Thermal evolution of defects in PLD grown ZnO samples was studied. Extensive out-diffusion of Zn into the sapphire substrate (~100 nm) was found at the ZnO/sapphire interface of the 900 °C annealed sample grown with oxygen, but the Zn-out-diffusion is limited to ~50 nm for the sample grown without oxygen. The results of the annealing and stoichiometric studies of the 584 cm^{-1} Raman line are compatible with the assignment of this line to oxygen vacancy. However, the result of the annealing study of the 560 cm^{-1} shows that it has higher thermal stability than that expected for Zn_i, and thus the previous literature assignment of this line to Zn_i is suspicious. Zn-vacancy related defects VZn-1, VZn-2, and VZn-3 having different microstructure are identified in the PLD grown samples. Annealing or growing the sample in oxygen would favor the formation of VZn-2. VZn-2 persisted after the 1100 °C annealing.

ACKNOWLEDGMENTS

This work was supported by the Research Grant Council, HKSAR under the GRF Project No. 703612P.

[1] Ü. Özgür, Ya. I. Alivov, C. Liu, A. Teke, M. A. Reshchikov, S. Doğan, V. Avrutin, S.-J. Cho, and H. Morkoç, J. Appl. Phys. **98**, 041301 (2005).
[2] D. C. Look, Phys. Status Solidi B **241**, 624 (2004).
[3] V. Avrutin, D. J. Silversmith, and H. Morkoç, Proc. IEEE **98**, 1269 (2010).
[4] A. Janotti and C. G. Van de Walle, Phys. Rev. B **76**, 165202 (2007).
[5] A. Janotti and C. G. Van de Walle, Rep. Prog. Phys. **72**, 126501 (2009).
[6] F. Oba, M. Choi, A. Togo, and I. Tanaka, Sci. Technol. Adv. Mater. **12**, 034302 (2011).
[7] M. D. McCluskey and S. J. Jokeia, J. Appl. Phys. **106**, 071101 (2009).
[8] F. Tuomisto, V. Ranki, K. Saarinen, and D. C. Look, Phys. Rev. Lett. **91**, 205502 (2003).
[9] F. Tuomisto, K. Saarinen, D. C. Look, and G. C. Farlow, Phys. Rev. B **72**, 085206 (2005).
[10] Z. Q. Chen, S. J. Wang, M. Maekawa, A. Kawasuso, H. Naramoto, X. L. Yuan, and T. Sekiguchi, Phys. Rev. B **75**, 245206 (2007).
[11] Z. Q. Chen, K. Betsuyaku, and A. Kawasuso, Phys. Rev. B **77**, 113204 (2008).
[12] G. Brauer, W. Anwand, D. Grambole, J. Grenzer, W. Skorupa, J. Čížek, J. Kuriplach, I. Procházka, C. C. Ling, C. K. So, D. Schulz, and D. Klimm, Phys. Rev. B **79**, 115212 (2009).
[13] J. C. Fan, C. Y. Zhu, S. Fung, C. D. Beling, Y. C. Zhong, K. S. Wong, Z. Xie, G. Brauer, W. Anwand, W. Skorupa, C. K. To, B. Yang, C. D. Beling, and C. C. Ling, J. Appl. Phys. **106**, 073709 (2009).
[14] C. K. To, B. Yang, S. C. Su, C. C. Ling, C. D. Beling, and S. Fung, J. Appl. Phys. **110**, 113521 (2011).
[15] F. A. Selim, M. H. Weber, D. Solodovnikov, and K. G. Lynn, Phys. Rev. Lett. **99**, 085502 (2007).
[16] R. Diggle, Phys. Rev. Lett. **23**, 579 (1969).
[17] B. Guo, Z. R. Qiu, and K. S. Wong, Appl. Phys. Lett. **82**, 2290 (2003).
[18] K. Vanheusden, C. H. Seager, W. L. Warren, D. R. Tallant, and J. A. Volgt, Appl. Phys. Lett. **68**, 403 (1996).
[19] X. L. Wu *et al.*, Appl. Phys. Lett. **78**, 2285 (2001).
[20] B. X. Lin, Z. X. Fu, and Y. B. Jia, Appl. Phys. Lett. **79**, 943 (2001).
[21] N. O. Korsunska, L. V. Borkovska, B. M. Bulakh, L. Yu Khomenkova, V. I. Kushnirenko, and I. V. Markevich, J. Lumin. **102–103**, 733 (2003).
[22] X. Q. Wei, B. Y. Man, M. Liu, C. S. Xue, H. Z. Zhuang, and C. Yang, Physica B **388**, 145 (2007).
[23] H. J. Fan, R. Scholz, F. M. Kolb, M. Zacharias, U. Gösele, F. Heyroth, C. Eiwenschmidt, T. Hempel, and J. Christen, Appl. Phys. A **79**, 1895 (2004).
[24] C. Li, J. Lv, S. Yao, J. Hu, and Z. Liang, Nuclear Instrum. Methods Phys. Res. B **295**, 11 (2013).
[25] D. Messerschmidt, K. Bratz, W. Gnehr, H. Romanus, J. Eberhardt, S. Nicolay, and C. Ballif, J. Appl. Phys. **115**, 094902 (2014).
[26] X. Xue, L. Liu, Z. Wang, and Y. Wu, J. Appl. Phys. **115**, 033902 (2014).
[27] J. F. Ziegler, J. P. Biersack, and U. Littmark, *The Stopping and Range of Ions in Solids* (Pergamon, New York, 1985).
[28] C. G. Van de Walle, Phys. Rev. Lett. **85**, 1012 (2000).
[29] L. S. Vlasenki and G. D. Watkins, Phys. Rev. B **72**, 035203 (2005).
[30] F. Tuomisto and I. Makkonen, Rev. Mod. Phys. **85**, 1583 (2013).
[31] L. W. Lu, C. K. So, C. Y. Zhu, C. J. Li, S. Fung, G. Brauer, W. Anwand, W. Skorupa, and C. C. Ling, Semicond. Sci. Technol. **23**, 095028 (2008).
[32] R. S. Wang, Q. L. Gu, C. C. Ling, and H. C. Ong, Appl. Phys. Lett. **92**, 042105 (2008).

[This article is copyrighted as indicated in the article. Reuse of AIP content is subject to the terms at: http://scitation.aip.org/termsconditions. Downloaded to] IP: 147.8.31.43 On: Mon, 26 Jan 2015 04:38:15